

Gravity wave–fine structure interactions: A reservoir of small-scale and large-scale turbulence energy

David C. Fritts,¹ Ling Wang,¹ and Joe Werne¹

Received 15 June 2009; revised 11 August 2009; accepted 26 August 2009; published 10 October 2009.

[1] A direct numerical simulation of gravity wave – fine structure interactions is performed to evaluate the effects of such a superposition on instability and turbulence for fine structure shears and a gravity wave (GW) amplitude that are individually stable. The superposition leads to deformations of the fine structure and GW fields that exhibit Kelvin-Helmholtz (KH) shear instabilities and turbulence extending over more than 20 buoyancy periods. KH instabilities occur on multiple scales, deplete the kinetic energy of the initial fine structure, and yield a layering of the potential temperature field resembling “sheet and layer” structures observed in the oceans and the atmosphere. The interactions have a much smaller effect on the GW amplitude. Such interactions among GWs and fine structure are likely ubiquitous throughout the atmosphere and oceans and may account for sporadic bursts of turbulence and its persistence in regions of apparent static and dynamic stability ($Ri > 1/4$). **Citation:** Fritts, D. C., L. Wang, and J. Werne (2009), Gravity wave–fine structure interactions: A reservoir of small-scale and large-scale turbulence energy, *Geophys. Res. Lett.*, 36, L19805, doi:10.1029/2009GL039501.

1. Introduction

[2] Observations throughout the atmosphere indicate a superposition of dynamical features exhibiting smaller and larger spatial scales in the velocity and potential temperature fields. In the stable boundary layer (SBL) and residual layer (RL), active, decaying, or fossil turbulence layers may be significantly less than a meter in depth [Muschinski and Wode, 1998; Balsley et al., 2003, 2006], while mean shears, the nocturnal low-level jet (LLJ), Kelvin-Helmholtz (KH) shear instabilities, and propagating or ducted gravity waves (GWs), among other processes, may occur on vertical scales as large as a km or more [Blackadar, 1957; Mahrt, 1985, 1989; Blumen et al., 2001; Mahrt and Vickers, 2002; Poulos et al., 2002; Fritts et al., 2003a]. Spatial scales of these dynamics increase with altitude, but still span several decades horizontally and vertically at altitudes extending into the mesosphere and lower thermosphere (MLT). At all altitudes, turbulence layers, the fine structure arising from turbulence decay, flow instabilities, GWs (and tidal and planetary waves at higher altitudes), and spatially-variable mean flows ensure superpositions, and interactions, of motions occurring on very disparate scales [Gossard et al., 1971; Luce et al., 2001; Gavrilov et al., 2005]. In particular,

we anticipate that larger-scale GWs (and KH, wave-wave interaction, or other instabilities) throughout the atmosphere (and tidal structures in the MLT) will influence the evolution, and the tendency towards instability and turbulence, of motions on all spatial scales. Despite the potential significance of these dynamics, direct numerical simulations (DNS) specifically addressing mutual GW-fine structure interactions and their effects have never been performed.

[3] Such influences were anticipated to occur via interactions of larger-scale GWs with existing smaller-scale turbulence or modulation of the local Richardson number, Ri , by larger-scale motions in previous theoretical studies and data analyses [Chimonas, 1972; Einaudi and Finnigan, 1981; Finnigan and Einaudi, 1981; Fua et al., 1982; Finnigan et al., 1984; Meillier et al., 2008]. Small-scale turbulence also occurs as a result of direct GW instability, both systematic two-dimensional (2D) wave-wave interactions and local three-dimensional (3D) instabilities, of the larger-scale motions in the absence of initial fine structure [Klostermeyer, 1991; Müller et al., 1986; Lombard and Riley, 1996; Sonmor and Klaassen, 1997; Fritts et al., 1998, 2006, 2009a, 2009b]. The consequences of such instabilities are expected to include large- and small-scale turbulence layers, sharp vertical gradients in turbulence quantities, and the remnants of such layers exhibiting potentially sharp positive potential temperature gradients, sustained small-scale overturning, and local Richardson numbers that typically approach $Ri \sim 0.25$ as these layers restratify [Werne and Fritts, 1999, 2001; Luce et al., 2001; Balsley et al., 2003; Fritts et al., 2003b; Gavrilov et al., 2005]. However, these expectations have not been confirmed by DNS of GW-fine structure interactions to date.

[4] While various authors have addressed the links between large-scale GW motions and small-scale turbulence employing observational or theoretical studies, the specific mechanisms by which GW motions modulate the small-scale flow and turbulence formation or intensity have remained elusive. Our purpose here is to demonstrate one mechanism involving the deformation of background fine structure in the velocity profile (with minimum Richardson number $Ri = 1/4$) by a GW that is significantly below “breaking” amplitude. Three DNS of a GW with and without superposed fine structure, and one of fine structure without a GW, each with the same initial noise spectrum, are performed that enable an initial exploration of these dynamics. A brief description of our numerical model is provided in Section 2. Results exhibiting the dynamics of small-scale turbulence generation and its evolution are described in Section 3. These suggest a tendency for more general superpositions to be unstable to small-scale shear instability for a broad range of initial conditions. A summary of these results, and a discussion of their possible implications for

¹Colorado Research Associates Division, NorthWest Research Associates, Boulder, Colorado, USA.

similar dynamics in more general flows are provided in Section 4.

2. Numerical Model and Problem Specification

[5] We solve the nonlinear Navier-Stokes equations subject to the Boussinesq approximation in a Cartesian domain that is aligned along the phase of the primary GW, as in previous studies by *Fritts et al.* [2003b, 2006, 2009a, 2009b]. Nondimensionalizing with respect to the GW vertical wavelength λ_z and the buoyancy period, $T_b = 2\pi/N$, these equations may be written as

$$\partial \mathbf{u} / \partial t + \mathbf{u} \cdot \nabla \mathbf{u} = -\nabla p + Ri_b \theta \mathbf{z} + Re^{-1} \nabla^2 \mathbf{u} \quad (1)$$

$$\partial \theta / \partial t + \mathbf{u} \cdot \nabla \theta = (PrRe)^{-1} \nabla^2 \theta \quad (2)$$

$$\nabla \cdot \mathbf{u} = 0 \quad (3)$$

where $\mathbf{u} = (u, v, w)$ is the total velocity vector, p is pressure, θ is total potential temperature, and the bulk Richardson number relating the length and time scales is $Ri_b = N^2 \lambda_z^2 / U^2 = 4\pi^2$. We assume a Reynolds number $Re = \lambda_z^2 / \nu T_b = 2 \times 10^5$ and a Prandtl number $Pr = \nu / \kappa = 1$. The value of Re for representative GW scales varies enormously from $\sim 10^8$ in the lower atmosphere to $\sim 10^4$ or less in the MLT. A $Pr = 1$ is assumed to yield uniform resolution requirements in the velocity and potential temperature fields. The velocity scale is $U = \lambda_z / T_b$, and other quantities have their standard definitions [*Fritts et al.*, 2009a].

[6] Alignment of the computational domain along the GW phase ensures a periodic solution for domains potentially much smaller than the GW horizontal wavelength. This “tilting” of the domain yields substantial computational efficiencies relative to periodic solutions in a horizontal domain, but it also imposes greater discretization of the larger-scale motions than in a larger computational domain. In this case, we assume an intrinsic frequency $\omega = N/10$ with uniform background stratification, yielding a domain tilted relative to horizontal by $\sim 5.7^\circ$.

[7] The new aspect of this DNS relative to our previous studies is fine structure in the velocity field $U_{FS}(\mathbf{z}) = U_{FS} \sin(m_{FS} z)$ having a maximum velocity shear $dU_{FS}/dz = m_{FS} U_{FS} = 2N$, such that the minimum background $Ri = 1/4$. We also assume a GW amplitude expressed as $a = u'/c = 0.5$, where $a = 1$ corresponds to insipient “convective” overturning. This results in a minimum $Ri \sim 1/8$ for the superposed GW and fine structure background at the least stable GW phase (with no GW shear) and $Ri \sim 0.16$ where the GW shear is maximum, respectively.

[8] A large Re was chosen to allow an Re_{KH} appropriate for possible Kelvin-Helmholtz (KH) shear instability within the fine structure modulated by the GW of $Re_{KH} \sim (U_{FS}/2)(\lambda_{zFS}/2\pi)/\nu \sim 1000$ or more, where $\lambda_{zFS} = 2\pi/m_{FS}$, such that small-scale KH instability can be vigorous and 3D when it arises at sufficiently large scales. To allow the description of both the prescribed GW and the background fine structure, we chose domain dimensions of $(X', Y', Z') = (1, 0.1, 1) \lambda$. This is sufficiently large to allow multiple initial KH instability and secondary instability structures in

the streamwise and spanwise directions for the fine structure specified. Our descriptions of these GW, KH, and turbulence dynamics require resolution of $(N_x, N_y, N_z) = (1600, 160, 1600)$ Fourier modes to resolve the turbulence inertial range. Other details of our numerical model are provided by *Fritts et al.* [2009a].

3. Results

[9] The evolution of the GW with background fine structure is displayed with streamwise-vertical (x, z) cross sections of total vorticity magnitude through the center of the computational domain for times from $t = 3$ to $13 T_b$ in Figure 1. Spanwise-vertical (y, z) cross sections are also shown at lower right at early times. Note the tilt of the (x, z) cross sections along the GW phase. These images illustrate three aspects of the initial development: 1) a deformation of the fine structure vorticity by the large-scale GW, 2) the appearance of small-scale shear instabilities in the most unstable GW phase that evolve rapidly over $\sim 1 T_b$, and 3) instability at significantly larger vertical scales than occur in the initial fine structure due to deformation by the GW. The deformation of the fine structure is due to the oscillatory GW velocities having components along, and normal to, the fine structure itself. Indeed, this “misalignment” of the GW and fine structure velocities is key to the distortion, and obviously depends on GW frequency. This yields divergent (convergent) vertical velocities and convergent (divergent) horizontal velocities at the GW phase initially at the center (upper/lower edge) of the domain (and moving downward with the GW phase motion thereafter). Divergent (convergent) vertical motions cause deeper (shallower) shear layers and larger (smaller) fine structure velocities because the fine structure vorticity is simply advected by the 2D flow in the absence of sources and sinks. With the same vorticity, a deeper shear layer has a larger velocity differential (see the initial streamwise velocity profiles in Figure 2, top left). The fine structure vorticity is largely conserved following the fluid motion (but also enhanced by $\sim 25\%$ due to the GW shears at alternating fine-structure phase) until KH shear instability occurs, and these instabilities exhibit depths and intensities that depend on the local Ri and Re of the fine structure. The minimum local Ri for the superposed GW and fine structure is initially $\sim 1/8$ at the least stable phase of the GW ($z = 0.75$ at $t = 0$ in Figure 2, top) and ~ 0.16 at the maximum GW shear ($z = 0.5$ at $t = 0$ in Figure 2, top). Fine structure deformation plays a central role in instability formation and intensity, as $Re_{KH} \sim U_{FS} \lambda_{zFS} / 4\pi\nu$ varies \sim quadratically with shear layer depth for constant vorticity, and because shear layers having $Re_{KH} > 1000$ exhibit strong instability and rapid 3D evolution for reasonable Ri , while those with $Re_{KH} \sim 300$ or less either remain 2D and viscously damped or are suppressed entirely. Thus, a combination of reduced minimum Ri and increased Re at this phase of the GW appears to explain the preferential occurrence of initial KH instability at these locations for the enhanced fine-structure shears.

[10] Shear instability arises first in fine structure shears for which Ri is reduced by the GW in the upper portion of the domain. As the GW causes convergent horizontal motions near the domain center, however, deeper and more vigorous instabilities accompany the overturning of these

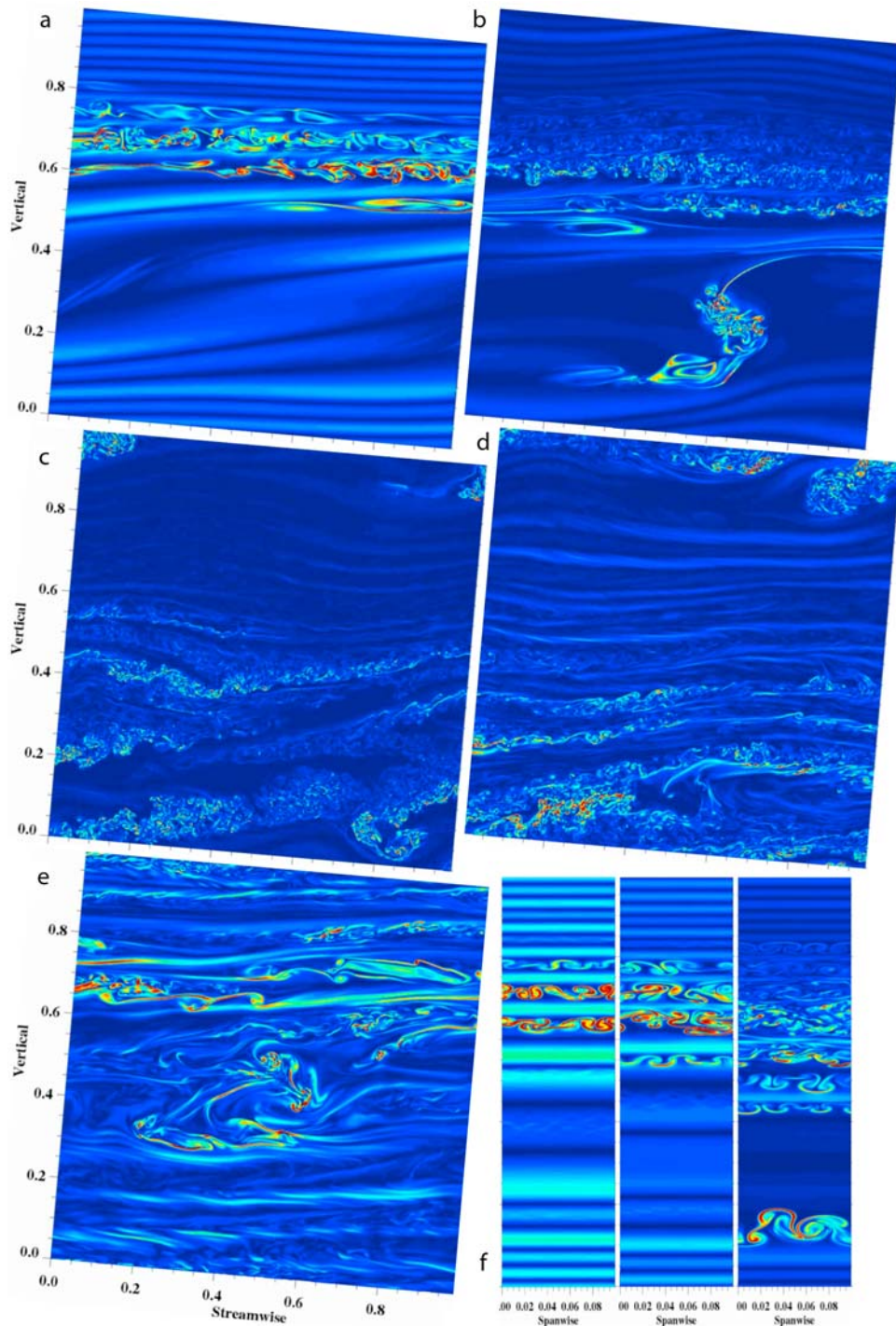


Figure 1. (a–e) The (x, z) cross sections and (f) (y, z) cross sections of vorticity magnitude through the center of the computational domain. Times are at $t = 3, 4, 6, 8$ and $13 T_b$ for the (x, z) cross sections and $t = 2.5, 3,$ and $4 T_b$ for the (y, z) cross sections. The vorticity is saturated at 40% of the maximum value, the domain is inclined along the GW phase, and group velocity is to the left and upward. The (y, z) cross sections are shown at ~ 2.5 times their true spanwise extent to exhibit the spanwise instability structures clearly. Note that turbulence arises on the fine-structure shears rather than due to GW overturning and instability in every case.

deeper shears. Instabilities evolve rapidly in both cases, expanding throughout the shear layers, until both shears and potential temperature gradients are largely eradicated (see the profiles at $t = 3$ to $4 T_b$ in Figure 2, top). The nature of the shear instability is inherently 3D at sufficiently large Re

even at the earliest times, as can be seen at several layers (having the same sign of vorticity) in the (y, z) cross section of vorticity magnitude in Figure 1. Indeed, the structures of the initial intensified vortex sheets within these shear layers are expected for shear layers at $Ri \sim 1/4$ for sufficiently

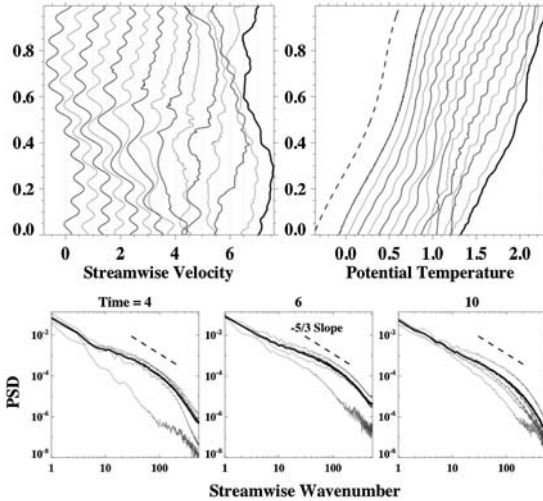


Figure 2. (top) Streamwise velocity and potential temperature profiles at $t = 0, 0.5, 1, 1.5, 2, 2.5, 3, 3.5, 4, 4.5, 5, 6, 8, 10,$ and $20 T_b$. Profiles are displaced by 0.5 ms^{-1} at left and 0.1 units at right. (bottom) Streamwise velocity spectra at $t = 4, 6,$ and $10 T_b$. Light lines are for 0.2λ altitude intervals; bold lines are the mean over the DNS volume. A $-5/3$ slope is shown in each panel. The inertial range is seen to shift to smaller scales with time. All spectra exhibit roll-off into the viscous range, suggesting that even the smallest spatial scales seen in Figure 1 are well resolved.

high Re due to the lack of coherent and stable KH vortex cores that arise only at much lower Ri . The initial instability structures also closely resemble the secondary instability structures arising initially in the exterior of KH billows at low Ri and high Re . The sinuous character of the vorticity sheets seen in all of the (y, z) cross sections in Figure 1 is due to counter-rotating streamwise-aligned vortices within these shear layers that advect the vorticity sheets up and down and stretch and intensify them between alternating streamwise-aligned vortices. These relatively coherent 3D vorticity structures quickly enable vortex interactions that drive enstrophy to smaller scales thereafter.

[11] Also seen at $t = 4 T_b$ in Figure 1 are streamwise variations in fine structure displacements near the upper and lower edges of the domain having the streamwise wavelength of the domain and a large-scale overturning event occupying $\sim 1/3$ of the vertical domain depth that arose from an individual shear layer. The streamwise variations in fine structure displacements are an indication that these dynamics have triggered excitation of a secondary GW having a much smaller horizontal wavelength ($\sim \lambda$), and that this emerging GW is playing a significant role in the modulation of the fine structure thereafter. We know this because the initial GW amplitude results in peak-to-peak vertical displacements of only $1/2\pi$ of the domain depth for $a = 0.5$, and this feature is ~ 2 times deeper.

[12] The large-scale overturning represents a deep accumulation of spanwise vorticity and a large Re enabling vigorous instability dynamics, including strong secondary and tertiary KH instability dynamics extending to very small spatial scales and late times (see the small-scale vorticity features at $z \sim 0.5$ to 0.6 at $t = 4$, at $z \sim 0.1$ to 0.3

and ~ 0.95 at $t = 8$, and at somewhat larger scales at $z \sim 0.6$ to 0.9 at $t = 13$ in Figure 1). Indeed, KH instabilities continue to form on multiple scales throughout the $>20 T_b$ duration of the simulation. Their wavelengths range from ~ 0.02 to 1λ , and their core dynamics are 2D or 3D, depending on the shear scales and magnitudes (and thus Ri and Re).

[13] As fine structure shear layers exhibit instability and 3D cascades of enstrophy to smaller scales, the initial fine structure variability in streamwise velocity is seen to disappear to a large degree (see Figure 2, top, at $t = 3 T_b$ and beyond). In contrast, fine structure is nonexistent in the potential temperature field at early times, but it arises both as a result of differential GW and fine structure advection and accompanying mixing within unstable shear layers. The former is the dominant mechanism while fine structure shears are strong (up to $t \sim 3 T_b$); the latter is dominant following widespread shear instability and mixing (after $t \sim 3 T_b$). At intermediate stages, fine structure in the velocity field has diminished significantly, but there remains residual fine structure in the potential temperature field arising from mixing that persists to late times. Indeed, this structure is very reminiscent of the “sheet and layer” structures often seen in the ocean thermocline, the atmospheric boundary layer, and the free atmosphere [Muschinski and Wode, 1998; Luce et al., 2001; Balsley et al., 2003; Gavrilov et al., 2005], and having KH instability as a cause, as initially suggested by Woods [1969], Posmentier [1977], Gossard et al. [1985], and Woodman and Chu [1989]. The GW, in contrast, is seen to decrease in amplitude by $<6\%$ over the $20 T_b$ duration of the DNS.

[14] Streamwise spectra of streamwise velocities derived from our DNS at $t = 4, 6,$ and $10 T_b$ are displayed in the lower panels of Figure 2. Individual spectra (thin lines) are for altitude intervals of 0.2λ depths; bold lines are means over the DNS volume. Turbulence is very weak at early times, with spectral amplitudes above streamwise wavenumbers ~ 10 maximizing at $t \sim 6 T_b$ and decaying at later times. Spectral amplitudes also fall sharply above wavenumbers of ~ 100 and exhibit much steeper slopes within the viscous range, especially at $t \sim 10 T_b$ and beyond. These spectra suggest that the small-scale structures discussed above are apparently well resolved, and that even the smallest-scale KH instabilities seen in the (x, z) cross sections of vorticity magnitude are well within the inertial range of turbulence at these times.

[15] We also performed three additional simulations to clarify the roles of the initial Ri and potential 2D GW instability in driving the turbulence dynamics discussed above. One described the large-scale GW with the same initial noise spectrum, but without the background fine structure. A second examined the evolution of the fine structure alone, with the same initial noise. Neither displayed any instability over the same time span, indicating that the dynamics discussed here are a consequence of the superposition, and mutual interaction, of the GW and the background fine structure. A third examined the same GW-fine structure interaction, but with weaker fine structure shears such that the initial superposed flow had a minimum $Ri = 1/4$ ($dU_{FS}/dz = m_{FS} U_{FS} = 1.4N$). This also yielded significant and persistent (but also less rapid and energetic, due to the smaller available kinetic energy) instability dynamics and turbulence, implying that an initial $Ri \geq 1/4$ is

not a reliable predictor of the absence of turbulence in flows exhibiting significant scale interactions.

4. Summary and Conclusions

[16] We describe an initial DNS of GW – fine structure interactions that reveals dramatic coupling of large- and small-scale motions. Initially stable fine structure shears are advected and deformed by a GW which is itself stable, while the fine structure modulates the GW velocity and potential temperature fields. These deformations initiate KH instabilities occurring at fine-structure scales that erode the shear layers and induce turbulence and mixing that may extend over far greater depths than the initial fine structure shear depths. Instabilities and turbulence arise on many spatial scales, persist for more than $20 T_b$ (2 GW periods), largely deplete the kinetic energy of the initial fine structure, and yield a layering of the potential temperature field resembling the “sheet and layer” structures that are well documented in the oceans and the atmosphere. Turbulence generation is dramatically different than that accompanying GW breaking and leaves the GW reduced in amplitude by $<6\%$ at $t = 20 T_b$. We suggest that such interactions among large-scale GWs and fine structure due to decaying turbulence or small-scale inertia-GWs must be ubiquitous throughout the atmosphere and oceans, due to the constant misalignment of high-frequency GW phase structures with background or lower-frequency shear flows, and the potential for fine-structure and GW deformation that these imply. We also expect that the detailed dynamics will be sensitive to the orientation of the fine structure vorticity. This is because GW deformation of spanwise vorticity will expand or contract shear layers through vorticity advection (but without changing the vorticity magnitude), while GW deformation of streamwise vorticity will also stretch or compress this vorticity (thus intensifying or weakening the associated shears). Finally, we suggest that such dynamics likely contribute to sporadic bursts of turbulence and its persistence in regions of high apparent static and dynamic stability ($Ri > 1/4$) at larger spatial scales.

[17] **Acknowledgments.** Support for this research was provided by NSF grants ATM-0836407, ATM-0737692, and ATM-0436703. We also acknowledge the DoD HPCMO for access to large computational resources without which these studies would have been impossible.

References

Balsley, B. B., R. G. Frehlich, M. L. Jensen, and Y. Meillier (2003), Extreme gradients in the nocturnal boundary layer: Structure, evolution, and potential causes, *J. Atmos. Sci.*, *60*, 2496–2508, doi:10.1175/1520-0469[2003]060 < 2496:EGITNB > 2.0.CO;2.

Balsley, B. B., R. G. Frehlich, M. L. Jensen, and Y. Meillier (2006), High-resolution in situ profiling through the stable boundary layer: Examination of the SBL top in terms of minimum shear, maximum stratification, and turbulence decrease, *J. Atmos. Sci.*, *63*, 1291–1307, doi:10.1175/JAS3671.1.

Blackadar, A. K. (1957), Boundary layer wind maxima and their significance for the growth of nocturnal inversions, *Bull. Am. Meteorol. Soc.*, *38*, 283–290.

Blumen, W., et al. (2001), Turbulence statistics of a Kelvin-Helmholtz billow event observed in the nighttime boundary layer during the CASES-99 field program, *Dyn. Atmos. Oceans*, *34*, 189–204, doi:10.1016/S0377-0265(01)00067-7.

Chimonas, G. (1972), The stability of a coupled wave-turbulence system in a parallel shear flow, *Boundary Layer Meteorol.*, *2*, 444–452, doi:10.1007/BF00821547.

Einaudi, F., and J. J. Finnigan (1981), The interaction between an internal gravity wave and the planetary boundary layer. Part I: The linear analysis, *Q. J. R. Meteorol. Soc.*, *107*, 793–806, doi:10.1256/smsqj.45403.

Finnigan, J. J., and F. Einaudi (1981), The interaction between an internal gravity wave and the planetary boundary layer. Part II: Effect of the wave on the turbulence structure, *Q. J. R. Meteorol. Soc.*, *107*, 807–832, doi:10.1256/smsqj.45404.

Finnigan, J. J., F. Einaudi, and D. Fua (1984), The interaction between an internal gravity wave and turbulence in the stably-stratified nocturnal boundary layer, *J. Atmos. Sci.*, *41*, 2409–2436, doi:10.1175/1520-0469[1984]041 < 2409:TIBAIG > 2.0.CO;2.

Fritts, D. C., S. Arendt, and O. Andreassen (1998), Vorticity dynamics in a breaking internal gravity wave. Part 2. Vortex interactions and transition to turbulence, *J. Fluid Mech.*, *367*, 47–65, doi:10.1017/S0022112098001633.

Fritts, D. C., et al. (2003a), Analysis of ducted motions in the stable nocturnal boundary layer during CASES-99, *J. Atmos. Sci.*, *60*, 2450–2472, doi:10.1175/1520-0469[2003]060 < 2450:AODMIT > 2.0.CO;2.

Fritts, D. C., C. Bizon, J. A. Werne, and C. K. Meyer (2003b), Layering accompanying turbulence generation due to shear instability and gravity wave breaking, *J. Geophys. Res.*, *108*(D8), 8452, doi:10.1029/2002JD002406.

Fritts, D. C., S. L. Vadas, K. Wan, and J. A. Werne (2006), Mean and variable forcing of the middle atmosphere by gravity waves, *J. Atmos. Sol. Terr. Phys.*, *68*, 247–265, doi:10.1016/j.jastp.2005.04.010.

Fritts, D. C., L. Wang, J. Werne, T. Lund, and K. Wan (2009a), Gravity wave instability dynamics at high Reynolds numbers. Part I: Wave field evolution at large amplitudes and high frequencies, *J. Atmos. Sci.*, *66*, 1126–1148, doi:10.1175/2008JAS2726.1.

Fritts, D. C., L. Wang, J. Werne, T. Lund, and K. Wan (2009b), Gravity wave instability dynamics at high Reynolds numbers. Part II: Turbulence evolution, structure, and anisotropy, *J. Atmos. Sci.*, *66*, 1149–1171, doi:10.1175/2008JAS2727.1.

Fua, D., et al. (1982), An analysis of wave-turbulence interaction, *J. Atmos. Sci.*, *39*, 2450–2463, doi:10.1175/1520-0469[1982]039 < 2450:AAOWTI > 2.0.CO;2.

Gavrilov, N. M., et al. (2005), Turbulence parameter estimations from high-resolution balloon temperature measurements of the MUTSI-2000 campaign, *Ann. Geophys.*, *23*, 2401–2413.

Gossard, E. E., D. R. Jensen, and J. H. Richter (1971), An analytical study of tropospheric structure as seen by high-resolution radar, *J. Atmos. Sci.*, *28*, 794–807, doi:10.1175/1520-0469[1971]028 < 0794:AASOTS > 2.0.CO;2.

Gossard, E. E., J. E. Gaynor, R. J. Zamora, and W. D. Neff (1985), Fines-structure of elevated stable layers observed by sounder and in situ tower sensors, *J. Atmos. Sci.*, *42*, 2156–2169, doi:10.1175/1520-0469[1985]042 < 2156:FOESLO > 2.0.CO;2.

Klostermeyer, J. (1991), Two- and three-dimensional parametric instabilities in finite amplitude internal gravity waves, *Geophys. Astrophys. Fluid Dyn.*, *61*, 1–25, doi:10.1080/03091929108229035.

Lombard, P. N., and J. J. Riley (1996), Instability and breakdown of internal gravity waves. I. Linear stability analysis, *Phys. Fluids*, *8*, 3271–3287, doi:10.1063/1.869117.

Luce, H., M. Crochet, and F. Dalaudier (2001), Temperature sheets and aspect sensitive radar echoes, *Ann. Geophys.*, *19*, 899–920.

Mahrt, L. (1985), Vertical structure and turbulence in the very stable boundary layer, *J. Atmos. Sci.*, *42*, 2333–2349, doi:10.1175/1520-0469[1985]042 < 2333:VSATIT > 2.0.CO;2.

Mahrt, L. (1989), Intermittency of atmospheric turbulence, *J. Atmos. Sci.*, *46*, 79–95, doi:10.1175/1520-0469[1989]046 < 0079:IOAT > 2.0.CO;2.

Mahrt, L., and D. Vickers (2002), Contrasting vertical structures of nocturnal boundary layers, *Boundary Layer Meteorol.*, *105*, 351–363, doi:10.1023/A:1019964720989.

Meillier, J., R. G. Frehlich, R. M. Jones, and B. B. Balsley (2008), Modulation of small-scale turbulence by ducted waves in the nocturnal boundary layer, *J. Atmos. Sci.*, *65*, 1414–1427, doi:10.1175/2007JAS2359.1.

Müller, P., G. Holloway, F. Henyey, and N. Pomphrey (1986), Nonlinear interactions among internal gravity waves, *Rev. Geophys.*, *24*(3), 493–536, doi:10.1029/RG024i003p00493.

Muschinski, A., and C. Wode (1998), First in situ evidence for coexisting submeter temperature and humidity sheets in the lower free troposphere, *J. Atmos. Sci.*, *55*, 2893–2906, doi:10.1175/1520-0469[1998]055 < 2893:FISEFC > 2.0.CO;2.

Posmentier, E. S. (1977), The generation of salinity fine structure by vertical diffusion, *J. Phys. Oceanogr.*, *7*, 298–300, doi:10.1175/1520-0485[1977]007 < 0298:TGOSFB > 2.0.CO;2.

Poulos, G. S., et al. (2002), CASES-99: A comprehensive investigation of the stable nocturnal boundary layer, *Bull. Am. Meteorol. Soc.*, *83*, 555–581, doi:10.1175/1520-0477[2002]083 < 0555:CACIOT > 2.3.CO;2.

- Sonmor, L. J., and G. P. Klaassen (1997), Toward a unified theory of gravity wave stability, *J. Atmos. Sci.*, *54*, 2655–2680, doi:10.1175/1520-0469[1997]054<2655:TAUTOG>2.0.CO;2.
- Werne, J. A., and D. C. Fritts (1999), Stratified shear turbulence: Evolution and statistics, *Geophys. Res. Lett.*, *26*, 439–442, doi:10.1029/1999GL900022.
- Werne, J. A., and D. C. Fritts (2001), Anisotropy in a stratified shear layer, *Phys. Chem. Earth*, *26*, 263–268.
- Woodman, R. F., and Y. Y.-H. Chu (1989), Aspect sensitivity measurements of VHF backscatter made with the Chung-Li radar: Plausible mechanisms, *Radio Sci.*, *24*, 113–125, doi:10.1029/RS024i002p00113.
- Woods, J. D. (1969), On Richardson's number as a criterion for laminar-turbulent-laminar transition in the ocean and atmosphere, *Radio Sci.*, *4*, 1289–1298, doi:10.1029/RS004i012p01289.

D. C. Fritts, L. Wang, and J. Werne, CORA, NWRA, 3380 Mitchell Lane, Boulder, CO 80301, USA. (dave@cora.nwra.com)